

Journal of Materials Chemistry C

Accepted Manuscript



This is an *Accepted Manuscript*, which has been through the Royal Society of Chemistry peer review process and has been accepted for publication.

Accepted Manuscripts are published online shortly after acceptance, before technical editing, formatting and proof reading. Using this free service, authors can make their results available to the community, in citable form, before we publish the edited article. We will replace this *Accepted Manuscript* with the edited and formatted *Advance Article* as soon as it is available.

You can find more information about *Accepted Manuscripts* in the [Information for Authors](#).

Please note that technical editing may introduce minor changes to the text and/or graphics, which may alter content. The journal's standard [Terms & Conditions](#) and the [Ethical guidelines](#) still apply. In no event shall the Royal Society of Chemistry be held responsible for any errors or omissions in this *Accepted Manuscript* or any consequences arising from the use of any information it contains.

ARTICLE

Graphene oxide vs. reduced graphene oxide as core substrate for core/shell-structured dielectric nanoplates with different electro-responsive characteristics

Cite this: DOI: 10.1039/x0xx00000x

Received 00th January 2012,
Accepted 00th January 2012

DOI: 10.1039/x0xx00000x

www.rsc.org/Ludan Li^a, Jianbo Yin^{a,*}, Yang Liu, and Xiaopeng Zhao^a

Not only the polarizability but also the polarization rate of particles is important to the electro-responsive electrorheological (ER) characteristic of particle suspensions. In this paper, we respectively use non-conducting graphene oxide (GO) and conducting reduced graphene oxide (r-GO) as core and use insulating SiO₂ as shell to prepare core/shell-structured dielectric nanoplates for the purpose of achieving optimum ER response to different electric stimuli. The morphology and structure of samples are characterized by scanning electron microscopy, transmission electron microscopy, atomic force microscopy, X-ray diffraction, thermogravimetric analysis, Raman spectroscopy, and X-ray photoelectronic spectroscopy. The conductivity and dielectric properties are measured by impedance analyzer and the electro-responsive ER characteristics of nanoplates dispersed in insulating oil are investigated by rheometer. It demonstrates that coating with SiO₂ can provide electrically insulating effect for GO or r-GO core, while GO vs. r-GO as core can induce distinctly different dielectric polarization response. Compared to GO/SiO₂, r-GO/SiO₂ shows significantly faster polarization rate due to the high conductivity of r-GO core. As a result, the r-GO/SiO₂ suspension exhibits high ER response to high-frequency AC electric fields, while the GO/SiO₂ suspension exhibits high ER response to DC or low-frequency AC electric fields. This different electro-responsive characteristic can be explained by the influence of polarization rate on interparticle interaction.

Introduction

Using an electric or a magnetic stimulus to control the rheological characteristics of fluids is very interesting because of the potential usage in the active control of conventional and intelligent devices.^{1,2} These fluids, whose rheology can be controlled by an external field, are referred as smart fluids. Electrorheological (ER) suspensions, consisting of polarizable particles in electrically insulating oil carrier, are a type of important smart fluids whose viscosity and viscoelastic properties can be tuned by an external electric field.³ Without an electric field, the particles are randomly dispersed in oil and the suspensions show a Newtonian fluid behavior. With an electric field, the dispersed particles are polarized and attract each other to form chain-like structures between two electrodes. The gap-spanning chain structures can largely increase the viscosity of suspensions within several milliseconds and the suspensions show a Bingham fluid behavior. When the electric field is removed, ER suspensions can rapidly go back to the initially low-viscous state. Because of the advantages including short response time, reversibility, and low power consumption,

ER suspensions have potential uses as electrical–mechanical interfaces of various devices in mechanical, biomedical and robotic fields.^{4,5} However, the conventional ER suspensions based on micro-size particles often subject to poor dispersion stability and low ER effect and, thus, the real application is still limited.^{6,7}

Recent works of using nanoparticles as the dispersed phase have promoted much experimental activity to develop non-conventional ER suspensions with improved dispersion stability and ER effect.⁸ In particular, compared to sphere-like particles, using elongated nanoparticles (e.g. nanofibers, nanotubes, and nanoplates) as the dispersed phase of ER suspensions has attracted significant interests due to enhanced properties.⁹ For example, Lin and Shan have reported that the suspension of carbon nanotubes exhibits much larger electrically induced viscosity than that of the suspension of glassy carbon spheres.^{9b} We have demonstrated that the suspension of nano-fibrous polyaniline has much stronger ER effect and lower particle settling compared to the suspension of granular polyaniline at the same volume fractions.^{9c} Wu et al. have prepared rod-like calcium titanyl oxalate with enhanced ER effect compared with

granular one.^{9g} The property enhancement has been considered to be related to the large aspect ratio morphology and anisotropic electrical properties of elongated particles, which have largely influenced the interparticle interaction and the hydrodynamic property of suspensions under the simultaneous effect of both electric and shearing fields.

Due to large aspect ratio, excellently electrical properties, and facile preparation, graphene and its oxide (graphene oxide) have also received growing attention as the active component or filler of electro-responsive ER suspensions.^{10,11} Pure graphene oxide (GO) can be directly used as the dispersed phase of ER suspensions due to its low conductivity.¹² But it is difficult to disperse pure GO in nonpolar oils (e.g. silicone oil and mineral oil) because of the hydrophilic nature of lots of oxygen-containing functional groups on GO. Therefore, more studies have concentrated on the ER effect of GO-based composites, such as GO/polyaniline, GO/polystyrene, GO/silica hybrid, GO-wrapped TiO₂, etc.¹¹ However, the composites are micro-size stacking particles and the large particle settling problem still needs to overcome. Contrary to GO, pure graphene is not able to be used as the dispersed phase of ER suspensions because its high conductivity easily causes current leaching and dielectric breakdown. To overcome this problem, we have proposed a strategy of coating insulating layer onto graphene and developed novel core/shell-structured graphene composite nanoplates for ER suspension application.¹⁰ The composite nanoplates possess not only large-aspect-ratio plate-like morphology but also decreased conductivity. These characters endow the graphene composite nanoplates with potential as the novel dispersed phase of non-conventional ER suspensions. In addition, because the structure and properties of core or shell can be controllably adjusted, the unique core/shell nano-architecture may be interesting to understand ER mechanism and achieve optimum ER response to different electric stimuli for special applications.

In this paper, for the purpose of achieving optimum ER response to different electric stimuli, we respectively use non-conducting GO and conducting reduced GO (r-GO) as core and use insulating SiO₂ as shell to prepare core/shell-structured dielectric nanoplates by a simple wet-chemical method. The formation of core/shell nanoplate structure is confirmed by scanning electron microscopy (SEM), transmission electron microscopy (TEM), atomic force microscopy (AFM), X-ray diffraction (XRD), thermogravimetric analysis (TGA), Raman spectroscopy, and X-ray photoelectronic spectroscopy (XPS). The conductivity and dielectric properties of nanoplates are measured by impedance analyzer and the ER characteristics of their suspensions in silicone oil are comparably investigated by rheological test under various electric fields. The results show that coating with SiO₂ can provide an electrically insulating effect for GO or r-GO core, while GO vs. r-GO as core can induce distinctly different dielectric polarization due to their different conductivity. As a result, GO/SiO₂ and r-GO/SiO₂ exhibit different ER response to DC and AC electric stimuli. This different electro-responsive characteristic can be explained by the influence of polarization rate on interparticle interaction.

Experimental section

Materials

Tetraethylorthosilicate (TEOS), ammonia, hydrazine, and natural graphite plates with mean size of ~20 μm were purchased from Sinopharm Chemical Reagent Co. Ltd. of China. Pluronic F-127 ((PEO)₁₀₆(PPO)₇₀(PEO)₁₀₆) was purchased from Aldrich. All the chemicals were of analytical grade and were used without further purification.

Preparation of GO/SiO₂ and r-GO/SiO₂ nanoplates

Firstly, GO was synthesized from natural graphite by an improved Hummers method.¹³ Simply, 18.0 g of KMnO₄ were added into a 9:1 mixture of concentrated H₂SO₄/H₃PO₄ (360:40 mL) under stirring and then 3.0 g of graphite flakes was added to form uniform suspension. The suspension was heated to 50 °C and stirred for 12 h. After that, the suspension was cooled to 4 °C and poured with 3 mL of 30% H₂O₂. The filtrate was centrifuged and the remaining yellow solid was washed in succession with 30% HCl solution several times. After further washing with water to pH=5-6 and drying in vacuum, GO powder was obtained. *Subsequently*, 30.0 mg of dry GO powder was dispersed into 100 mL of ethanol containing 1.2 g Pluronic F-127 by ultrasonic agitation for 30 min at frequency of 40 kHz and power of 100 W. Here, Pluronic F127 as the amphiphilic copolymer adheres to the surface of GO and facilitates the heterogeneous nucleation of TEOS. *Then*, 4.0 mL of ammonia and 8.0 mL of water were respectively added into the dispersion to form yellow transparent colloid dispersion. After that, 20 mL of ethanol containing 2.0 mL of TEOS was added dropwise into the above GO colloid dispersion under stirring. After stirring for 12 h at 30 °C, grey precipitate was formed. *Finally*, the precipitate was centrifugally separated and washed with hot ethanol several times to remove Pluronic F-127 and get resulting plate-like GO/SiO₂ powder. Yield: ~0.6 g. The weight ratio of GO to SiO₂ is ~1:20 according to TGA result.

The r-GO/SiO₂ nanoplates were prepared by reducing GO/SiO₂ in hydrazine solution. Typically, 0.3 g of GO/SiO₂ was dispersed into 30 mL of water containing 1.5 mL hydrazine by ultrasonic agitation. After heating treatment for 2 h at 95 °C, black precipitate was formed. The precipitate was centrifugally separated and washed with ethanol several times to obtain resulting plate-like r-GO/SiO₂ powder. Yield: ~0.25 g. The weight ratio of r-GO to SiO₂ is ~1:18 according to TGA result. In addition, pure r-GO could also be obtained by reducing pure GO (15 mg) in hydrazine solution (1.5 mL hydrazine in 30 mL water) by the same process.

Preparation of ER suspensions

GO/SiO₂ and r-GO/SiO₂ nanoplates were dried at 100 °C in vacuum for 48 h and then were suspended into dimethyl silicone oil (KF-96, 50 Cst, Shin-Etsu Chemical Co. Ltd.). The suspensions were treated for 30 min by ultrasonic agitation at frequency of 40 kHz and power of 100 W in order to fully disperse the nanoplates into silicone oil. The volume fraction

(ϕ) of nanoplates in suspensions is defined by the ratio of the nanoplate volume (V_p) to the total volume (V) of suspensions. The nanoplate volume is defined by $V_p = m_p / \rho_p$, where m_p is the nanoplate mass and ρ_p is the nanoplate density. Here, ρ_p is measured by displacement of water in pycnometer. During density measurement, the pycnometer was placed in an ultrasonic cleaning bath and connected with a vacuum pump. After ultrasonication under reduced pressure for 30 s to remove residual air in powder and make water fully wet the powder, the density was measured. The value of ρ_p of GO/SiO₂ is 1.59 g/cm³, which is slightly lower than 1.64 g/cm³ of r-GO/SiO₂.

Characterization and measurements

The morphology of samples was observed by a scanning electron microscopy (SEM, JSM-6700F), transmission electron microscopy (TEM, FEI Tecnai F30 G²), and atomic force microscopy (AFM, Dimension Icon). The dilute nanoplate/ethanol dispersion was dropped on the lacey support film for TEM observation. The crystal structure of samples was determined by a powder X-ray diffraction pattern (XRD, Philips X'Pert Pro) with a CuK α irradiation at 40 kV/35 mA. The thermal decomposition of samples was determined by a thermogravimetric analysis (TGA, Netzsch STA449F3) with a heating rate of 10 °C/min within the temperature range of 30–800 °C in air. The surface composition of samples was analyzed by an X-ray photoelectron spectroscopy (XPS, Thermo Scientific K-Alpha) with a monochromatic AlK α source. All XPS spectra were corrected by the C1s line at 284.6 eV. The chemical state of samples, especially for GO vs. r-GO core, was clarified by Raman spectroscopy on a Micro-Raman spectrometer (Raman, invia) at 532 nm.

The DC conductivities of pure GO, GO/SiO₂ and r-GO/SiO₂ were measured by a two-point method on a digital high ohmmeter (Keithley 6517B). Prior to measuring, the powder was compressed into pellet and then silver electrodes were deposited on both sides. The DC conductivity of pure r-GO was measured by a four-point method (RTS-8) on compressed pellet.

The dielectric properties of nanoplates in suspensions were measured by an impedance analyzer (HP 4284A) in the frequency range of 20 – 10⁶ Hz using a measuring fixture (HP 16452A) for liquids. 1 V of bias electrical potential was applied to suspensions during measurement. It was so small that no chain structures was formed within suspensions, thus we could get the true behavior of interfacial polarization of nanoplates and make an equitable comparison of different samples.

The ER characteristics of suspensions were measured by a stress-controlled rheometer (Thermal-Haake RS600) with a parallel plate system (diameter = 35 mm, gap = 1.0 mm), DC and AC high-voltage generators, and an oil bath system. The flow curves of shear stress vs. shear rate were measured by the controlled shear rate (CSR) mode within 0.1 - 1000 s⁻¹ at room temperature. Before each measurement, we presheared the suspensions for 60 s at 300 s⁻¹ and then applied electric fields for 30 s to ensure the formation of equilibrium chain structures before shearing. The static yield stress (τ_s), which is defined as the stress that allows a solidified ER suspension to start to flow,

was approximately obtained with the shear stress in the low shear rate region according to the flow curves. The dynamic yield stress (τ_d) was obtained by extrapolating the flow curves to zero shear rate with the Bingham fluid model as shown in the following equation (1):

$$\tau = \tau_d + \eta_{pl} \dot{\gamma} \quad (1)$$

where, τ_d is the dynamic yield stress, η_{pl} is the plastic viscosity and $\dot{\gamma}$ is the shear rate.¹⁴

Results and discussion

Fig. 1 shows the schematic diagram of the preparation of the core-shell structured GO/SiO₂ and r-GO/SiO₂ nanoplates. Firstly, the GO colloid (Fig. 1(a)) was prepared. Then, SiO₂ shell was coated on the surface of GO sheets by the hydrolyzation and condensation of TEOS under the help of amphiphilic copolymer. After washing and dry, the resulting GO/SiO₂ is obtained and its appearance is grey powder (Fig. 1(b)). After hydrazine reduction, the grey GO/SiO₂ powder is changed into black one (Fig. 1(c)) due to GO core is reduced into r-GO core.

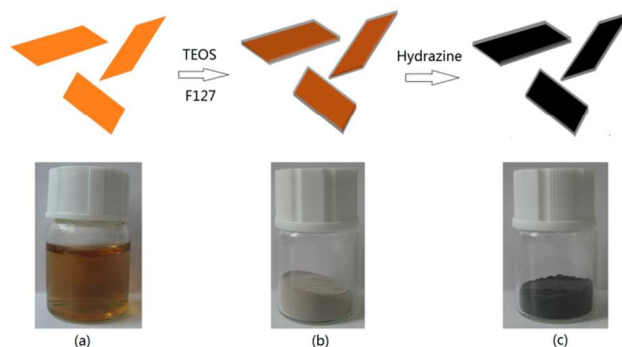


Fig. 1 Schematic preparation process of the core-shell structured GO/SiO₂ and r-GO/SiO₂ nanoplates and the corresponding photograph of the appearance of samples: (a) GO colloid; (b) GO/SiO₂; (c) r-GO/SiO₂.

Fig. 2 shows the SEM and TEM images of typical GO/SiO₂ (GO: SiO₂ = ~1:20) and r-GO/SiO₂ (r-GO: SiO₂ = ~1:18) samples. Pure GO is very thin with thickness of ~1.0 nm (see AFM image in Fig. 3(a)) and it can be well dispersed in water or ethanol, but it is easy to stack into large agglomerate after dry (see Fig. S1(a) in the ESI†). As shown in Fig. 2(a), however, the GO/SiO₂ shows free-standing plate-like morphology after dry, indicating that coating with SiO₂ has well restrained the stacking of GO. The lateral size of plates is 1-5 μ m and the total thickness is ~30 nm (inset in Fig. 2(a) and AFM image in Fig. 3(b)). Thus, the thickness of SiO₂ shell is ~15 nm. Pure r-GO, which is obtained by reducing GO by hydrazine, is also stacking agglomerate (Fig. S1(b) in the ESI†) but it is very difficult to re-disperse into water or ethanol due to strong π - π interaction between layers.¹⁵ Therefore, we cannot directly use pure r-GO to prepare r-GO/SiO₂ but use hydrazine to reduce GO/SiO₂ into r-GO/SiO₂. As shown in Fig. 2(b), the r-GO/SiO₂ obtained by reducing GO/SiO₂ by hydrazine still

maintains free-standing nanoplate morphology. Its lateral size and thickness are similar to those of the GO/SiO₂ (inset in Fig. 2(b) and AFM image in Fig. 3(c)). Furthermore, no free SiO₂ particles are observed from the SEM, TEM and AFM images of GO/SiO₂ or r-GO/SiO₂ and the surface of GO or r-GO is uniformly covered by amorphous SiO₂ according to the TEM images in Fig. 2(c) and (d). This can be attributed to the fact that GO sheets facilitate the heterogeneous nucleation of TEOS during hydrolyzation and condensation with the help of amphiphilic Pluronic F127 copolymer. In absence of GO in reaction, we only get sphere-like SiO₂ particles, also supporting this point. In addition, the selected-area electron diffraction (SAED) pattern of GO/SiO₂ shows weak six-fold symmetry diffraction spots (marked by arrows in inset of Fig. 2(c)), which are similar to the SAED of carbon rings in GO.¹⁶ We consider that these diffraction spots should be originated from the GO core and their weak intensity can be ascribed to the coverage of amorphous SiO₂ shell. It also hints the formation of core/shell structure in the GO/SiO₂ nanoplates. The SAED spots of r-GO/SiO₂ is much weaker compared to those of GO/SiO₂ (see inset of Fig. 2(d)). This may be attributed to the decrease of the size of in-plane sp² domains due to the reduction of GO by hydrazine and the reestablishment of graphene network after removing oxygen functional groups.¹⁷

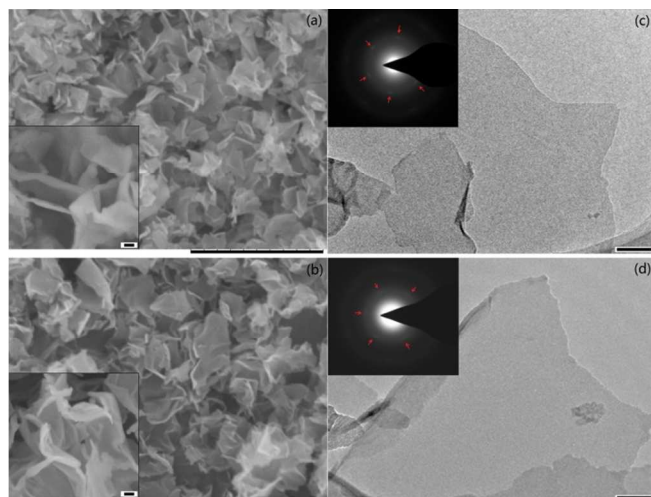


Fig. 2 SEM images of samples: (a) GO/SiO₂ and (b) r-GO/SiO₂; TEM and SAED (inset) images of samples: (c) GO/SiO₂ and (d) r-GO/SiO₂ (Scale bar = 5 μm for (a) and (b); Scale bar = 200 nm for insets in (a) and (b); Scale bar = 100 nm for (c) and (d)).

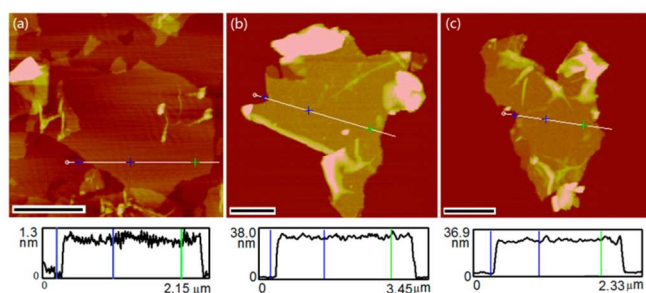


Fig. 3 AFM images of samples: (a) GO; (b) GO/SiO₂; (c) r-GO/SiO₂ (Scale bar = 1 μm for (a), (b) and (c)).

Fig. 4 shows the XRD pattern of samples. Pure GO shows a low-angle diffraction peak at ~9.5° corresponding to (002) plane of GO stacking (Fig. 4(a)).¹³ After coating with SiO₂, the 9.5° diffraction peak disappears and the sample only shows a broad peak at ~22.0° corresponding to amorphous structure of SiO₂ (Fig. 4(c)). This indicates that coating with SiO₂ has restrained the stacking of GO, which is in accordance with the SEM observation. Pure r-GO shows an abroad strong diffraction peak at ~24.0° and a weak diffraction peak at ~43.7°, corresponding to the (002) and (100) planes of graphite, respectively (Fig. 4(b)).¹⁸ It indicates that GO is reduced into r-GO by hydrazine solution and form graphite stacking due to strong π-π interaction between layers. The r-GO/SiO₂ also only shows a broad peak at ~22.0° corresponding to amorphous SiO₂ and the diffraction peak of the (002) plane of graphite does not appear (Fig. 4(d)). It also indicates that the r-GO core is not restacking due to coating with SiO₂ shell.

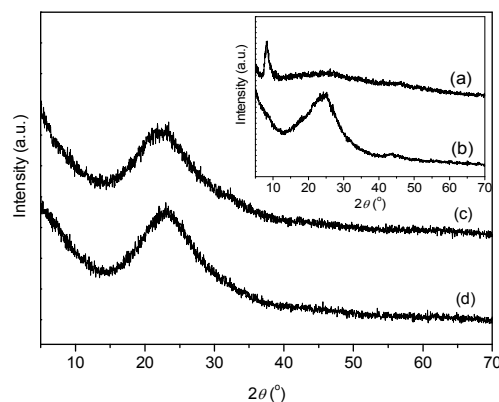


Fig. 4 XRD patterns of samples: (a) GO; (b) r-GO; (c) GO/SiO₂; (d) r-GO/SiO₂.

Fig. 5 shows the TGA trace of samples under air atmosphere. Pure GO shows a two-step weight loss at ~200 °C and 450-550 °C (Fig. 5(a)). The first one can be attributed to the pyrolysis of oxide functional groups, while the second one can be attributed to the combustion of bulk carbon material.¹⁹ Pure r-GO, which is obtained by reducing GO by hydrazine, mainly exhibits a large single-step weight loss at 400-600 °C due to the combustion of bulk carbon and does not show significant weight loss at ~200 °C due to the pyrolysis of oxide functional groups (Fig. 5(b)). This indicates that GO is reduced into r-GO according to the previous report.²⁰ As shown in Fig. 5(c), the GO/SiO₂ shows an approximate two-step weight loss at 100-250 °C due to the removal of physical water and the pyrolysis of oxide functional groups in GO core, 300-500°C due to the stimulus removal of GO core and small amount of residual organic in SiO₂ shell. As shown in Fig. 5(d), however, the r-GO/SiO₂ shows a broad single-step weight loss at 300-600 °C, which can be due to the stimulus removal of r-GO core and small amount of residual organic in SiO₂ shell. In particular, no significant weight loss at lower temperature than 300 °C indicates that the core in r-GO/SiO₂ has been deoxygenated.

Therefore, using hydrazine treatment can not only reduce pure GO into r-GO but also reduce the GO core in GO/SiO₂ into r-GO core. To further verify this, we also characterize it by XPS and Raman spectra in the following section. In addition, by comparing the weight loss of GO/SiO₂ and r-GO/SiO₂ with that of pure SiO₂ (Fig. 5(e)), we can get the weight ratio of GO to SiO₂ and r-GO to SiO₂ is ~1:20 and ~1:18, respectively. It is close to the initial ratio of raw materials in the reaction, indicating a high yield.

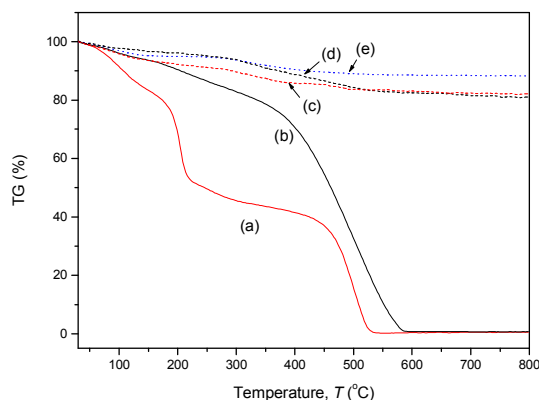


Fig. 5 TGA curves of samples: (a) GO; (b) r-GO; (c) GO/SiO₂; (d) r-GO/SiO₂; (e) SiO₂.

The surface composition of samples is clarified by XPS spectra. As shown in Fig. 6(a), pure GO mainly contains C and O elements. The O content is 35.42 at% (see Table 1). The deconvolution of the core-level C1s XPS spectrum of GO shows types of carbon bonds including C=C/C–C (284.6 eV), C–O (287.1 eV), and C=O (289.5 eV) (see Fig. S2(a) in the ESI†). After coating with SiO₂, the intensity of C1s peak decreases but the intensity of O1s peak increases (Fig. 6(c)). At the same time, the Si2s and Si2p peaks appear. Meanwhile, the O/Si atomic ratio is ~1.86, which is close to 2. It indicates that the surface of GO sheets should be mainly covered by SiO₂. As shown in Fig. 6(b), pure r-GO obtained by reducing GO by hydrazine contains C, O, and small amount of N elements. Compared to GO, the O content in r-GO is decreased to ~18.40 at%. At the same time, the intensity of the C=C/C–C bond (284.6 eV) increases but the intensity of oxidized carbon bonds (C–O at 286.9 eV and C=O at 288.5 eV) noticeably decreases (see Fig. S2(b) in the ESI†). These indicate that GO has been deoxygenated to form r-GO.²¹ As shown in Fig. 6(d), the intensity of C1s peak decreases but the Si2s and Si2p peaks appear in the r-GO/SiO₂. The O/Si atomic ratio is ~1.78, which is close to 2, indicating that the coverage on the surface of r-GO is also SiO₂.

Table 1. Surface element content analysis of samples.

Samples	C (at%)	O (at%)	N (at%)	Si (at%)
GO	64.58	35.42	-	-
GO/SiO ₂	40.53	38.65	-	20.83
r-GO	77.85	18.40	3.76	-
r-GO/SiO ₂	37.35	40.12	-	22.53

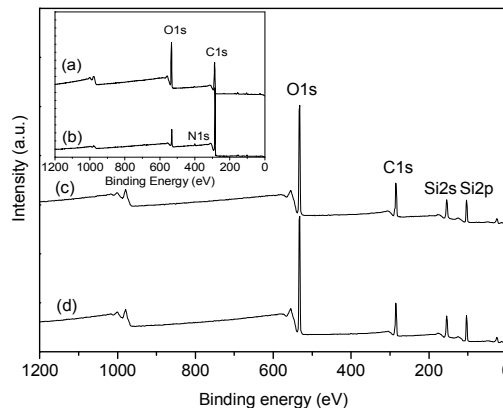


Fig. 6 XPS spectra of samples: (a) GO; (b) r-GO; (c) GO/SiO₂; (d) r-GO/SiO₂.

The chemical state of GO and r-GO cores in the core/shell nanoplates is clarified by Raman spectroscopy because it is a very effective tool to determine the structural variation of carbonaceous materials. As shown in Fig. 7(a) and (b), pure GO and r-GO show the D band at ~1350 cm⁻¹ due to the defect-induced breathing mode of sp² rings and the G band at ~1590 cm⁻¹ due to the first order scattering of the E_{2g} phonon of sp² carbon atoms.²² Besides D and G bands, the GO/SiO₂ and r-GO/SiO₂ (see Fig. 7(c) and (d)) also show weak feature peak of SiO₂ at ~490 cm⁻¹ corresponding to the siloxane ring breathing mode,²³ indicating the coexistence of GO or r-GO and SiO₂ in the core/shell composite nanoplates. In addition, the relative intensity ratio of D band to G band (I_D/I_G) is a measure of disorder degree and is inversely proportional to the average size of sp² clusters.²⁴ Compared to that ($I_D/I_G=0.93$) of GO, I_D/I_G of r-GO is increased to 1.03. The similar slight increase of the I_D/I_G ratio of GO after hydrazine reduction has also been observed in previous reports.^{25,26} It reflects that more graphitic domains are formed and the sp² cluster number is increased, indicating the conversion of GO into r-GO.²⁷ Similarly, $I_D/I_G=1.04$ for the r-GO/SiO₂, which is higher than that ($I_D/I_G=0.93$) of the GO/SiO₂, also indicating that the GO core in nanoplates has been well converted into r-GO core. In order to verify the conversion of GO core into r-GO core more clearly, we further remove the SiO₂ shell by etching GO/SiO₂ and r-GO/SiO₂ in HF solution. The deconvolution of the C1s XPS spectrum (see Fig. S3 in the ESI†) shows that the residual core material of GO/SiO₂ after HF etching possesses C=C/C–C (284.6 eV), C–O (286.9 eV), and C=O (289.0 eV) bonds, which are in accordance with the GO form. However, the C=C/C–C bond (284.6 eV) of the residual core material of r-GO/SiO₂ after etching is significantly strong and the oxidized carbon bonds (C–O and C=O) are weak, which clearly indicates that the core of r-GO/SiO₂ is the r-GO form.²¹

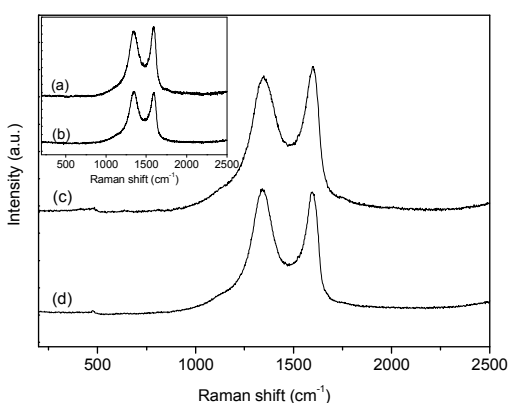


Fig. 7 Raman spectra of samples: (a) GO; (b) r-GO; (c) GO/SiO₂; (d) r-GO/SiO₂.

The conductivity of pure GO is $\sim 8.4 \times 10^{-6}$ S/cm and that of r-GO is ~ 5.6 S/cm. After coating with SiO₂, the conductivity is decreased to $\sim 6.5 \times 10^{-10}$ S/cm for the GO/SiO₂ and $\sim 1.7 \times 10^{-9}$ S/cm for the r-GO/SiO₂. The large decrease in conductivity indicates that SiO₂ shell has been well coated onto GO or r-GO surface and it is providing an effectively electrically insulating effect for GO or r-GO core. The dielectric spectra of GO/SiO₂ and r-GO/SiO₂ when dispersed in silicone oil are presented in Fig. 8. The dielectric parameters (Table 2) are determined by fitting the spectra by the following Cole-Cole equation:

$$\varepsilon^* = \varepsilon' + i\varepsilon'' = \varepsilon'_\infty + \frac{\varepsilon'_0 - \varepsilon'_\infty}{1 + (j\omega\tau)^{1-\alpha}} \quad (2)$$

where, ε^* is the complex permittivity, ε'_0 and ε'_∞ are the limit values of the relative permittivity at the frequencies below and above the relaxation frequency, respectively, ω is an angle frequency, τ is a dielectric relaxation time, and α is the scattering degree of relaxation time. $\Delta\varepsilon' = \varepsilon'_0 - \varepsilon'_\infty$ respects the magnitude of achievable polarization and τ reflects the rate of polarization. These two parameters are important to ER effect because the former is related to the magnitude of interparticle interaction, while the latter is related to the stability of interparticle interaction and the reorganization of chain structures under the simultaneous effect of both electric and shearing fields.²⁸⁻³⁰ As seen, both suspensions exhibit interfacial polarization with a clear dielectric relaxation peak within measured frequency range. The $\Delta\varepsilon'$ value of the r-GO/SiO₂ suspension is about 0.92, which is slightly larger than 0.90 of the GO/SiO₂ suspension. However, the τ value of the latter is 4.5×10^{-7} s, which is significantly faster than 3.2×10^{-4} s of the former. This indicates that the achievable polarizability of r-GO/SiO₂ is slightly larger than that of GO/SiO₂, but its polarization rate is much faster compared to GO/SiO₂. The faster polarization rate can be attributed to the fact that the core substrate in r-GO/SiO₂ has higher conductivity compared to GO/SiO₂ because other factors, such as particle morphology, shell thickness, and electric parameter of surrounding medium, are similar for both nanoplate suspensions.³¹

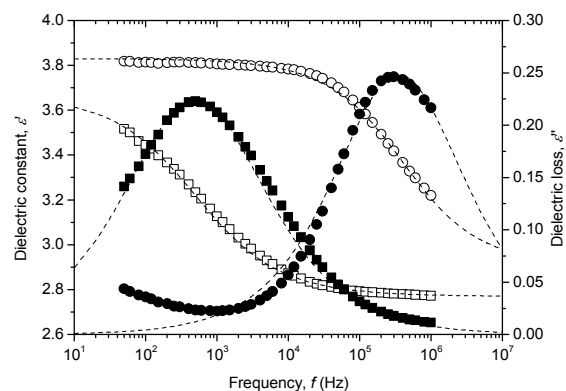


Fig. 8 Dielectric constant (open symbol) and loss factor (solid symbol) as a function of frequency for GO/SiO₂ suspension (square symbol) and r-GO/SiO₂ suspension (circle symbol). The dash line is fitted by the Cole-Cole equation ($\phi = 3$ vol%, $T = 23$ °C).

Table 2. Conductivity and dielectric properties of GO/SiO₂ and r-GO/SiO₂ suspensions ($\phi = 3$ vol%, $T = 23$ °C).

Samples	ε'_0	ε'_∞	$\Delta\varepsilon'^a$	ε''^b	f_{\max} (kHz)	τ (s) ^c	σ_p (S/cm) ^d
GO/SiO ₂	3.67	2.77	0.90	0.23	0.5	3.2×10^{-4}	$\sim 6.5 \times 10^{-10}$
r-GO/SiO ₂	3.83	2.91	0.92	0.25	300	4.5×10^{-7}	$\sim 1.7 \times 10^{-9}$

^a The dielectric constant increment of suspensions calculated by $\Delta\varepsilon' = \varepsilon'_0 - \varepsilon'_\infty$; ^b The dielectric loss factor of suspensions at the frequency (f_{\max}) of dielectric relaxation peak; ^c The dielectric relaxation time of suspensions calculated by $\tau = 1/(2\pi f_{\max})$; ^d The DC conductivity of nanoplates.

Therefore, based on the characterizations above, by a simple wet-chemical method, not only core/shell-structured nanoplates with a non-conducting GO core but also nanoplates with a conducting r-GO core have been obtained. The SiO₂ shell has provided an effectively insulating effect for GO or r-GO core, while GO vs. r-GO as core has induced significantly different polarization response. Since not only the polarizability but also the polarization rate of particles is important to ER effect, the different polarization response is expected to induce different ER response to different electric stimuli. In the following, we comparably investigate the ER characteristic of GO/SiO₂ vs. r-GO/SiO₂ when subjected to DC and AC electric fields.

Fig. 9(a) and (b) respectively shows the flow curves of shear stress vs. shear rate for the GO/SiO₂ suspension under DC electric fields and high-frequency AC electric fields with 1 kHz. In absence of electric fields, the suspension is shearing thin but does not possess an obvious yield stress. The off-field viscosity is ~ 0.25 Pas at 1000 s⁻¹. When electric fields are applied, the suspension exhibits a significant increase in shear stress, so-called ER effect, and behaves like a plastic material with a yield stress. This can be attributed to the formation of gap-spanning chain structures between electrodes due to the polarization and electrostatic interaction between nanoplates, which is hindering flow. As the electric field strength increases, the ER effect increases due to the increase of electric field-induced interparticle interaction. Meanwhile, the leaking current density of GO/SiO₂ suspension is ~ 1.5 $\mu\text{A}/\text{cm}^2$ at 2 kV/mm of DC electric field. Concerning the effect of different electric stimuli, however, there is distinctly difference in the

rheogram. Under DC electric fields, the GO/SiO₂ suspension not only possesses a high yield stress but also maintains a stable flow behavior in wide shear rate region after the appearance of yield stress. The widely accepted flow model for ER suspensions, i.e. the Bingham fluid model,³² is able to fit the flow curves as shown by the dash lines in Fig. 9(a). Under high-frequency AC electric fields, however, the yield stress of suspension is significantly lower compared to that under DC electric fields. For example, the yield stress is about 200 Pa at 2 kV/mm of AC electric field, which is much lower than 680 Pa at 2 kV/mm of DC electric field. At the same time, the shear stress tends to continuously climb up with shear rate after the appearance of yield stress and the flow curves departure from the Bingham model in the low shear rate region (see the dash lines in Fig. 9(b)). These reflect that the ER effect of GO/SiO₂ degrades on exposure to high-frequency AC electric stimuli.

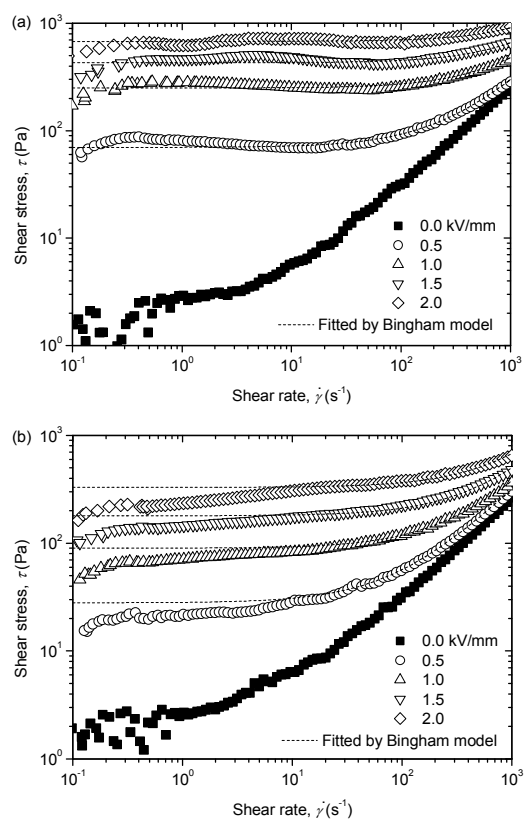


Fig. 9 Flow curves of shear stress vs. shear rate for GO/SiO₂ suspension under DC electric fields (a) and under AC electric fields with frequency of 1 kHz (b) ($\phi = 3$ vol%, $T = 23$ °C).

Fig. 10(a) and (b) respectively shows the flow curves of shear stress vs. shear rate for the r-GO/SiO₂ suspension under DC electric fields and high-frequency AC electric fields with 1 kHz. In absence of electric fields, the suspension is also shearing thin and does not possess a yield stress. The off-field viscosity is ~ 0.24 Pas at 1000 s⁻¹, which is very close to that of the GO/SiO₂ suspension. This can be attributed to the fact that r-GO/SiO₂ almost has the same morphology, size, density, and surface property as GO/SiO₂. When electric fields are applied, the r-GO/SiO₂ suspension also exhibits a significant ER effect

and the ER effect increases with the increase of electric field strength. Meanwhile, the leaking current density of r-GO/SiO₂ suspension is ~ 3.5 $\mu\text{A}/\text{cm}^2$ at 2 kV/mm of DC electric field. Compared with the GO/SiO₂ suspension, however, the r-GO/SiO₂ suspension exhibits significant different rheogram. The first difference concerns the rheogram under DC electric fields. Different from the stable flow behavior of GO/SiO₂ suspension in Fig. 9(a), although the yield stress of the r-GO/SiO₂ suspension is high, the shear stress tends to decline as a function of shear rate to a minimum value after the appearance of yield stress and then increases again (see Fig. 10 (a)). The similar shear stress decrease at a low shear rate region has also been observed in other ER materials under DC electric fields.³³ The Bingham fluid model is not able to fit the flow curves, especially in the low shear rate region as shown by the dash lines in Fig. 10(a). The second difference is that the ER effect of the GO/SiO₂ suspension degrades on exposure to high-frequency AC electric fields, while the ER effect of the r-GO/SiO₂ suspension seems to become better. As shown in Fig. 10(b), under AC electric fields with 1 kHz, the r-GO/SiO₂ suspension not only maintains high yield stress but also shows a stable flow behavior after the appearance of yield stress. The different rheogram above clearly indicates that the r-GO/SiO₂ has a distinctly different ER response from the GO/SiO₂, which has resulted in different interparticle interaction.

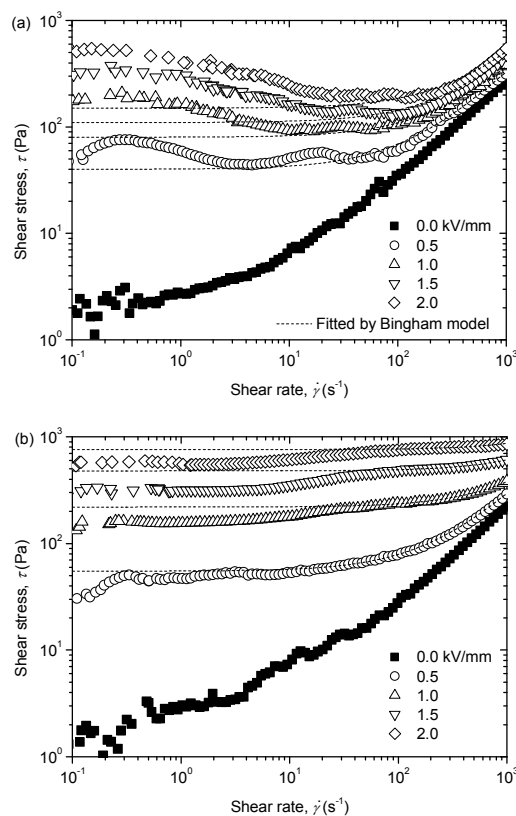


Fig. 10 Flow curves of shear stress and shear viscosity vs. shear rate for r-GO/SiO₂ suspension under DC electric fields (a) and under AC electric fields with frequency of 1 kHz (b) ($\phi = 3$ vol%, $T = 23$ °C).

It is known that the rheological behavior of ER suspensions is dominated by the competition between the interparticle electrostatic interaction induced by electric fields and the hydrodynamic interaction induced by shearing fields.³² The interparticle electrostatic interaction tends to maintain gap-spanning chain structures and hinder the flow, while the hydrodynamic interaction tends to destroy chain structures and promote the flow. At low shear deformation, the hydrodynamic interaction is too small to overcome the electrostatic interaction and, as a result, the chain structures are not distorted and ER suspensions approximately behave as an elastic solid with a well-defined yield stress. As the shear rate increases and exceeds yield point, ER suspensions start to flow and the flow behavior depends on the balanced situation where the chain structures are continuously broken and rebuilt by the competition between interparticle electrostatic interaction and hydrodynamic interaction. In this case, not only polarizability but also polarization rate of particles is important because the polarization rate is related to the stability of interparticle interaction and the reorganization of chain structures under simultaneous effect of both electric and shearing fields.³² Under DC electric fields, it has been proposed that ER suspensions with a polarization rate corresponding to the relaxation frequency within 10^2 – 10^5 Hz are appropriate for achieving a good rheological performance. Too slow or too fast polarization rate is not favorable to the stability and the reorganization of chain structures during flow because that too slow polarization rate easily results in insufficient particle polarization during flow, while too fast polarization rate easily results in the increase of repulsive interaction between particles due to the difference between the polarization direction and the direction connecting two particles.^{30a} From Fig. 8, we can see that the polarization rate of GO/SiO₂ suspension is $\sim 3.2 \times 10^{-4}$ s and the corresponding relaxation frequency is ~ 500 Hz, which is appropriate for DC electric fields. Thus, the particles can maintain sufficient polarizability and stable interparticle interaction and, as a result, the suspension shows a stable flow behavior in wide shear rate region as shown in Fig. 9(a). The polarization rate of r-GO/SiO₂ suspension is $\sim 4.5 \times 10^{-7}$ s and the corresponding relaxation frequency is ~ 300 kHz, which exceeds the proposed frequency range of 10^2 – 10^5 Hz for DC electric stimuli. Thus, the repulsive interaction between particles will increase with the increase of shear deformation rate and the chain structures start to become unstable and, as a result, the shear stress decreases as a function of shear rate after the appearance of yield stress as shown in Fig. 10(a). Under high-frequency AC electric fields, however, it requires ER suspensions to possess faster polarization rate for achieving a good rheological performance because the reorganization of the destroyed chain structures require ER particles to have a faster polarization rate than under DC electric fields. Therefore, in the presence of high-frequency AC electric fields, the polarization rate of GO/SiO₂ is too slow to induce sufficient particle polarization and, as a result, the interparticle interaction and the ER effect decrease as shown in Fig. 9(b). But the fast polarization rate of r-GO/SiO₂ becomes favorable to maintain strong and stable interparticle interaction under high-frequency

AC electric fields and, as a result, its ER effect is strong and the flow curves become stable as shown in Fig. 10(b). High yield stress and stable flow behavior in a wide shear rate region are very important to the real application of ER suspensions.¹⁴ In terms of the rheogram above, it is noted that the GO/SiO₂ suspension is suitable for the application under DC or low-frequency AC electric stimuli, while the r-GO/SiO₂ suspension is suitable for the high-frequency AC electric stimuli.

To better compare the ER response of GO/SiO₂ and r-GO/SiO₂ to different electric stimuli, we further obtain the static yield stress (τ_s) and the dynamic yield stress (τ_d) as a function of the electric field strength and frequency from rheogram. The static yield stress corresponds to the stress making ER suspensions start to flow and it characterizes the strength of suspensions at the yield point. The dynamic yield stress is defined as the stress making ER suspensions continuously flow and it characterizes the strength of suspensions in the flow regime.³⁴

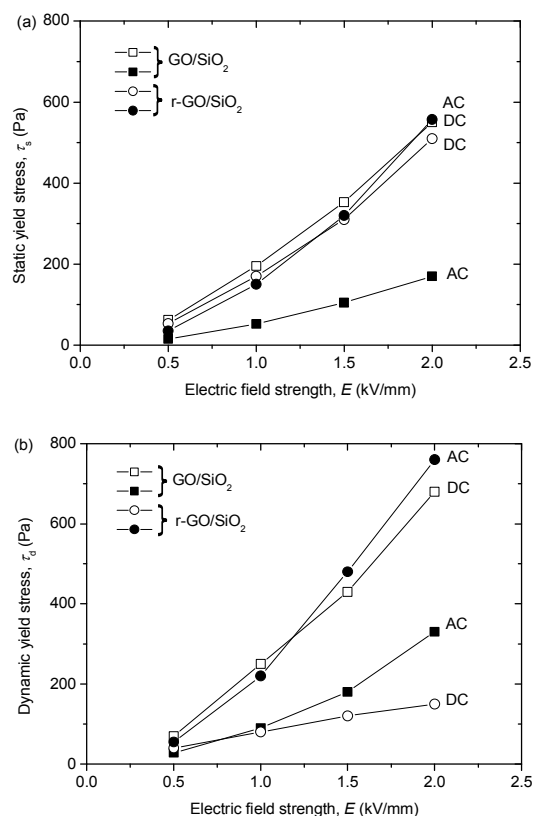


Fig. 11 Static yield stress (a) and dynamic yield stress (b) as a function of the electric field strength for GO/SiO₂ suspension (square symbol) and r-GO/SiO₂ suspension (circle symbol) under DC electric fields (open points) and AC electric fields with frequency of 1 kHz (solid points) ($\phi = 3$ vol%, $T = 23$ °C).

Fig. 11(a) and (b) respectively plots the values of static yield stress and dynamic yield stress as a function of electric field strength under DC and high-frequency AC electric fields. It is found that the static and dynamic yield stresses of both suspensions increase with electric field strength, as expected for

ER suspensions. On exposure to different electric stimuli, however, they show a different change. For the GO/SiO₂ suspension, both static and dynamic yield stresses are high under DC electric fields, indicating that the GO/SiO₂ suspension has high strength or ER effect not only at the yield point but also in the flow regime. Meanwhile, the magnitude of dynamic yield stress is higher than that of static yield stress at the same field strength. For example, the value of dynamic yield stress is ~680 Pa and the value of static yield stress is ~585 Pa at 2 kV/mm of DC electric field. This can be attributed to the fact that the static yield stress is the shear stress required to fracture the field-induced chain structures in their weakest point, while the dynamic yield stress is the one needed to continuously break all aggregates of chain structures.²⁸ Under high-frequency AC electric fields, however, both static and dynamic yield stresses of GO/SiO₂ suspension decrease significantly, indicating the degradation of ER effect. The reason for this can be ascribed to the slow polarization rate of GO/SiO₂, which results in the decline of achievable polarizability at high-frequency electric fields according to the dielectric analysis in Fig. 8.

For the r-GO/SiO₂ suspension, the static yield stress is high but the dynamic yield stress is obviously low under DC electric fields. For example, the value of static yield stress is ~578 Pa but the value of dynamic yield stress is only ~150 Pa at 2 kV/mm of DC electric field. This indicates that the r-GO/SiO₂ suspension has a high strength at yield point but the field-induced strength becomes weak after yield. The reason for this can be ascribed to that the static yield stress is mainly related to polarizability of particles when no shearing field, while the dynamic yield stress is related to both polarizability and polarization rate of particles under simultaneous effect of both electric and shearing fields.^{25a} Under DC electric fields, the high achievable polarizability of r-GO/SiO₂ can induce strong interparticle interaction, but its fast polarization rate is unfavorable to maintain stable interparticle interaction in the presence of both electric and shearing fields because too fast polarization rate easily results in the increase of repulsive interaction between particles with the increase of shear deformation rate. Therefore, the r-GO/SiO₂ suspension has a high strength before or at yield point but the weak strength in the flow regime. Under high-frequency AC electric fields, however, the r-GO/SiO₂ suspension shows not only high static yield stress but also high dynamic yield stress. It indicates that the r-GO/SiO₂ suspension not only possesses high field-induced strength or ER effect at yield point but also maintains high strength or ER effect in the flow regime under high-frequency AC stimuli. The phenomenon is different from that of the GO/SiO₂ suspension. The reason for this can also be attributed to the fast polarization rate of r-GO/SiO₂, which starts to become favorable to the ER effect under high-frequency AC electric fields because the reorganization of destroyed chain structures requires ER particles to have a faster polarization rate than under DC electric fields in order to match the frequency of external stimuli.

Fig. 12 (a) and (b) respectively plots the values of static yield stress and dynamic yield stress as a function of electric field frequency at 1.5 kV/mm. As observed, GO vs. r-GO as core

does induce distinctly different ER response to different electric stimuli. For the GO/SiO₂ suspension, both static yield stress and dynamic yield stress are high at DC or low-frequency AC electric fields but they tend to decrease on exposure to high-frequency AC electric fields. This can be explained by the dielectric analysis that shows the achievable polarizability of GO/SiO₂ is large in low-frequency range, while the polarizability declines with the increase of frequency due to slow polarization rate. For the r-GO/SiO₂ suspension, the static yield stress almost maintains constant as a function of electric field frequency within measured range. This can be attributed to the fact that the r-GO/SiO₂ can maintain a relatively high polarizability in a wide frequency range as shown in Fig. 8. However, the dynamic yield stress of r-GO/SiO₂ suspension is low at DC and low-frequency AC electric fields but it increases with electric field frequency and tends to become saturate at high frequency. It indicates that the field-induced strength in the flow regime is enhanced as the electric field frequency increases and this can be attributed to that the polarization rate of r-GO/SiO₂ gradually matches with the frequency of external stimuli and becomes favorable to the stability of interparticle interaction and the reorganization of destroyed chain structures. Therefore, the rheological results clearly indicate that use non-conducting GO as core can prepare core/shell-structured dielectric nanoplates with excellent ER response to DC or low-frequency AC electric stimulus, while using conducting r-GO can prepare dielectric nanoplates with excellent ER response to high-frequency AC electric stimulus.

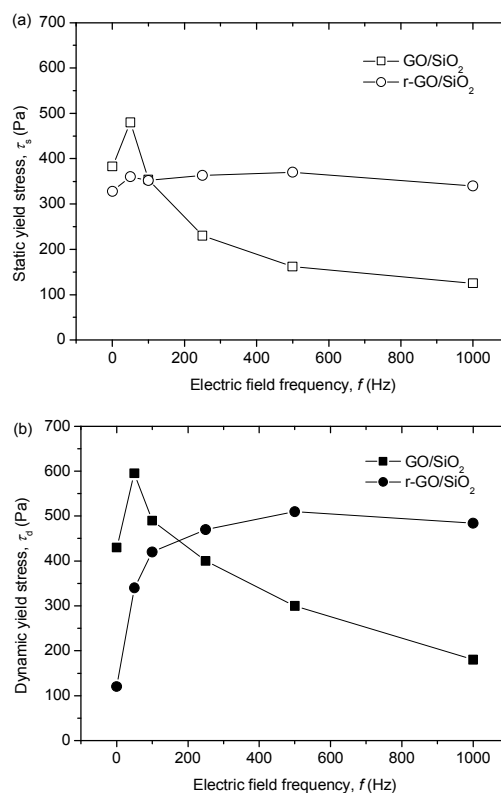


Fig. 12 Static yield stress (a) and dynamic yield stress (b) as a function of the electric field frequency for GO/SiO₂ suspension (square symbol) and r-GO/SiO₂ suspension (circle symbol) at 1.5 kV/mm ($\phi = 3$ vol%, $T = 23$ °C).

Finally, it is noted that the ER effect of GO/SiO₂ or r-GO/SiO₂ depends on the SiO₂ thickness or the weight ratio of GO to SiO₂ or r-GO to SiO₂. The ER effect of GO/SiO₂ decreases with the increase of SiO₂ thickness or the decrease of weight ratio of GO to SiO₂. This is attributed to the decrease of achievable polarizability with increase of SiO₂ thickness. The ER effect of r-GO/SiO₂ shows the maximum at the appropriate SiO₂ thickness or the weight ratio of r-GO to SiO₂ (i.e. r-GO: SiO₂ = ~1:18). This is attributed to the fact that the r-GO core is of high conductivity. Too thin SiO₂ shell cannot provide an effectively electrical insulating for it and thus the large leaking current results in the degradation of ER effect, while too thick SiO₂ shell also results in the appearance of single SiO₂ particles and the decrease of achievable polarizability. However, it is also noted that the off-field viscosity of GO/SiO₂ or r-GO/SiO₂ suspensions increases with the decrease of SiO₂ thickness or the increase of weight ratio of GO to SiO₂ or r-GO to SiO₂ at the same particle volume fraction. Therefore, an appropriate SiO₂ thickness is important to versatile ER performance, including a high ER efficiency but a relatively low off-field viscosity. In addition, it should be pointed out that, compared to the conventional core/shell-structured ER particles with hard core,³⁵ the GO or r-GO core in the present nanoplates is flexible and thus it may be easily breakable when the SiO₂ shell is thin. After cyclic rheological tests, however, we note that the ER effect and current density of the nanoplate suspensions maintain unchanged. This indicates that the morphology and structure of GO/SiO₂ and r-GO/SiO₂ nanoplates are not easily breakable under the stimulus effect of electric and shearing fields. When subjected to a strong ultrasonic treatment, the lateral size of nanoplates is found to slightly decrease but the current density of suspensions is almost unchanged. This indicates that the plate morphology is slightly breakable under the strong ultrasonic field but the core/shell structure is still robust.

Despite the ER effect between GO/SiO₂ and r-GO/SiO₂ shows a different dependence on the SiO₂ thickness or the weight ratio of GO to SiO₂ or r-GO to SiO₂, the ER response of GO/SiO₂ or r-GO/SiO₂ with different SiO₂ thickness shows similar dependence on electric field frequency. The GO/SiO₂ with different SiO₂ thickness all show high ER response to DC or low-frequency AC electric fields, while the r-GO/SiO₂ with different SiO₂ thickness all show high ER response to high-frequency AC electric fields. This is attributed to the fact that, although the achievable polarizability of GO/SiO₂ or r-GO/SiO₂ decreases with the SiO₂ thickness, the polarization rate (or the dielectric relaxation time) of GO/SiO₂ or r-GO/SiO₂ does not nearly change with the SiO₂ thickness. It also hints that the polarization rate of nanoplates is mainly dominated by the conductivity of GO or r-GO core rather than SiO₂ shell because the SiO₂ shell has small difference in electrical and dielectric properties with silicone oil carrier.

Conclusions

By a wet-chemical method, we have prepared core/shell-structured nanoplates with a non-conducting GO core and with a conducting r-GO core and then used them as novel dispersed

phase of smart ER suspensions. It has demonstrated that coating with SiO₂ can provide electrically insulating for GO or r-GO core, while GO vs. r-GO as core can induce distinctly different dielectric polarization response. Compared to GO/SiO₂, r-GO/SiO₂ shows significantly faster polarization rate due to the high conductivity of r-GO core. The rheological results have shown that the GO/SiO₂ nanoplate suspension exhibits high ER response to DC or low-frequency AC electric fields, while the r-GO/SiO₂ nanoplate suspension exhibits high ER response to high-frequency AC electric fields. The different electro-responsive characteristic can be explained by the influence of polarization rate on interparticle interaction. Our present results are not only interesting to understand ER mechanism but also providing a way to develop novel nanoplate-based ER suspensions with optimum response to different electric stimuli.

Acknowledgements

This work is supported by the National Natural Science Foundation of China (no. 51272214) and NPU Foundation for Fundamental Research (no. JC20120247).

†**Electronic supplementary information (ESI) available:** SEM images of pure GO and r-GO; the deconvolution of the core-level C1s XPS spectrum of pure GO and r-GO; the deconvolution of the C1s XPS spectrum of the residual core materials of GO/SiO₂ and r-GO/SiO₂ after HF etching.

Notes and references

^a Smart Materials Laboratory, Department of Applied Physics, Northwestern Polytechnical University, Xi'an 710129, P. R. China. Fax: 86 29 88491000; Tel: 86 29 88431662; E-mail: jbyin@nwpu.edu.cn

1. T. C. Halsey, *Science*, 1992, **258**, 761.
2. J. de Vicente, D. J. Klingenberg and R. Hidalgo-Alvarez, *Soft Matter*, 2011, **7**, 3701.
3. W. J. Wen, X. X. Huang and P. Sheng, *Soft Matter*, 2008, **4**, 200.
4. J. P. Coulter, K. D. Weiss and J. D. Carlson, *J. Intell. Mater. Syst. Struct.*, 1993, **4**, 248.
5. P. Sheng and W. J. Wen, *Annu. Rev. Fluid Mech.*, 2012, **44**, 143.
6. T. Hao, *Adv. Mater.*, 2001, **13**, 1847.
7. H. J. Choi and M. S. Jhon, *Soft Matter*, 2009, **5**, 1562.
8. (a) W. J. Wen, X. X. Huang, S. H. Yang, K. Q. Lu and P. Sheng, *Nat. Mater.*, 2003, **2**, 727; (b) K. Q. Lu, R. Shen, X. Z. Wang, G. Sun and W. J. Wen, *Int. J. Mod. Phys. B*, 2005, **19**, 1065; (c) G. J. Cao, M. Shen and L. W. Zhou, *J. Solid State Chem.*, 2006, **179**, 1565; (d) J. Y. Hong, E. Kwon and J. Jang, *Soft Matter*, 2009, **5**, 951.
9. (a) J. B. Yin and X. P. Zhao, *Nanotechnology*, 2006, **17**, 192; (b) C. Lin and J. W. Shan, *Phys. Fluids*, 2007, **19**, 121702; (c) J. B. Yin, X. P. Zhao, X. Xia, L. Q. Xiang and Y. P. Qiao, *Polymer*, 2008, **49**, 4413; (d) J. B. Yin, X. Xia, L. Q. Xiang and X. P. Zhao, *Carbon*, 2010, **48**, 2958; (e) Y. D. Liu, F. F. Fang and H. J. Choi, *Mater. Lett.*, 2010, **64**, 154; (f) J. B. Yin, X. Xia, L. Q. Xiang and X. P. Zhao, *J. Mater. Chem.*, 2010, **20**, 7096; (g) J. H. Wu, T. Jin, F. H. Liu, J. J. Guo, P. Cui, Y. C. Cheng and G. J. Xu, *J. Mater. Chem. C*, 2014, **2**, 5629.

10. (a) J. B. Yin, X. X. Wang, R. T. Chang and X. P. Zhao, *Soft Matter*, 2012, **8**, 294; (b) J. B. Yin, R. T. Chang, Y. J. Shui and X. P. Zhao, *Soft Matter*, 2013, **9**, 7468; (c) J. B. Yin, Y. J. Shui, R. T. Chang and X. P. Zhao, *Carbon*, 2012, **50**, 5247; (d) Y. Z. Dong, Y. Liu, J. B. Yin and X. P. Zhao, *J. Mater. Chem. C*, 2014, **2**, 10386.
11. (a) W. L. Zhang and H. J. Choi, *Soft Matter*, 2014, **10**, 6601; (b) W. L. Zhang, B. J. Park and H. J. Choi, *Chem. Commun.*, 2010, **46**, 5596; (c) W. L. Zhang, Y. D. Liu and H. J. Choi, *J. Mater. Chem.*, 2011, **21**, 6916; (d) W. L. Zhang and H. J. Choi, *Langmuir*, 2012, **28**, 7055; (e) J. B. Yin, Y. J. Shui, Y. Z. Dong and X. P. Zhao, *Nanotechnology*, 2014, **25**, 045702
12. (a) J. Hong and J. Jang, *Soft Matter*, 2012, **8**, 7348; (b) W. L. Zhang, Y. D. Liu, H. J. Choi and S. G. Kim, *ACS Appl. Mater. Interfaces*, 2012, **4**, 2267.
13. D. C. Marcano, D. V. Kosynkin, J. M. Berlin, A. Sinitskii, Z. Z. Sun, A. Slesarev, L. B. Alemany, W. Lu and J. M. Tour, *ACS Nano*, 2010, **4**, 4806.
14. K. D. Weiss and J. D. Carlson, *J. Intell. Mater. Syst. Struct.*, 1993, **4**, 13.
15. D. Li, M. B. Müller, S. Gilje, R. B. Kaner and G. G. Wallace, *Nat. nanotech.*, 2008, **3**, 101.
16. K. H. Liao, A. Mittal, S. Bose, C. Leighton, K. A. Mkhoyan and C. W. Macosko, *ACS Nano*, 2011, **5**, 1253.
17. H. Li, G. Zhu, Z. Liu, Z. Yang and Z. Wang, *Carbon*, 2010, **48**, 4391.
18. S. Park and J. An, *Carbon*, 2011, **49**, 3019
19. S. Niyogi, E. Bekyarova, M. E. Itkis, J. L. McWilliams, M. A. Hamon and R. C. Haddon, *J. Am. Chem. Soc.*, 2006, **128**, 7720.
20. S. Park, J. An, R. D. Piner, I. Jung, D. Yang, A. Velamakanni, S. T. Nguyen and R. S. Ruoff, *Chem. Mater.*, 2008, **20**, 6592.
21. Z. Zhang, F. Xiao, Y. Guo, S. Wang and Y. Liu, *ACS Appl. Mater. Interfaces*, 2013, **5**, 2227
22. K. N. Kudin, B. Ozbas, H. C. Schniepp, R. K. Prud'homme, I. A. Aksay and R. Car, *Nano Lett.*, 2008, **8**, 36
23. B. A. Morrow and D. T. Molapo, *Infrared studies of chemically modified silica*. In: H. E. Bergna and W. O. Roberts (Eds.), *Colloidal Silica: Fundamentals and Applications*, Boca Raton: CRC Press, 2005, p. 287–310.
24. C. Navarro, R. T. Weitz, A. M. Bittner, M. Scolari, A. Mews, M. Burghard and K. Kern, *Nano Lett.*, 2007, **7**, 3499.
25. S. Kim, S. H. Ku, S. Y. Lim, J. H. Kim and C. B. Park, *Adv. Mater.*, 2011, **23**, 2009.
26. Y. Xu, H. Bai, G. Lu, C. Li and G. Shi, *J. Am. Chem. Soc.*, 2008, **130**, 5856.
27. (a) Y. Xu, H. Bai, G. Lu, C. Li and G. Shi, *J. Am. Chem. Soc.*, 2008, **130**, 5856; (b) S. Stankovich, D. A. Dikin, R. D. Piner, K. A. Kohlhaas, A. Kleinhammes, Y. Jia, Y. Wu, S. T. Nguyen and R. S. Ruoff, *Carbon*, 2007, **45**, 1558.
28. W. L. Zhang, Y. D. Liu and H. J. Choi, *J. Mater. Chem.*, 2011, **21**, 6916.
29. (a) H. Block, J. P. Kelly, A. Qin and T. Watson, *Langmuir*, 1990, **6**, 6; (b) H. Block and P. Rattray, *Recent developments in ER fluids*. In: O. Havelkako and F. E. Filisko (Eds.), *Progress in electrorheology*. New York: Plenum Press, 1995. p. 19-42.
30. (a) F. Ikazaki, A. Kawai, K. Uchida, T. Kawakami, K. Edmura, K. Sakurai, H. Anzai and Y. Asako, *J. Phys. D: Appl. Phys.*, 1998, **31**, 336; (b) T. Hao, A. Kawai and F. Ikazaki, *Langmuir*, 1998, **14**, 1256. (c) A. Kawai, Y. Ide, A. Inoue and F. Ikazaki, *J. Chem. Phys.*, 1998, **109**, 4587.
31. C. Huang and Q. M. Zhang, *Appl. Phys. Lett.*, 2003, **82**, 3502.
32. M. Parthasarthy and D. J. Klingenberg, *Mater. Sci. Eng. R*, 1996, **17**, 57.
33. (a) Y. D. Liu and H. J. Choi, *Soft Matter*, 2012, **8**, 11961; (b) M. S. Cho, Y. H. Cho, H. J. Choi and M. S. Jhon, *Langmuir*, 2003, **19**, 5875.
34. M. T. López-López, A. Gómez-Ramírez, L. Rodríguez-Arco, J. D. G. Durán, L. Iskakova and A. Zubarev, *Langmuir*, 2012, **28**, 6232.
35. (a) Y. D. Liu, X. Quan, B. Hwang, Y. K. Kwon and H. J. Choi, *Langmuir*, 2014, **30**, 1729; (b) J. H. Wu, F. H. Liu, J. J. Guo, P. Cui, G. J. Xu and Y. C. Cheng, *Colloids Surf. A*, 2012, **410**, 136.

Graphic abstract

Using non-conducting graphene oxide vs. conducting reduced graphene oxide as the core substrate of core/shell-structured dielectric nanoplates can induce significantly different polarization response and smart electrorheological characteristic to different electric stimuli.

